

Response to electrons and pions of the calorimeter for the CHORUS experiment

E. Di Capua^a, M. Ferroni^a, C. Luppi^a, S. Ricciardi^a, B. Saitta^{a,1}, P. Zucchelli^{a,2},
S. Buontempo^b, A.G. Cocco^b, A. Ereditato^{b,*}, G. Fiorillo^b, F. Garufi^b, F. Marchetti-Stasi^b,
M. Messina^b, P. Migliozi^b, V. Palladino^b, P. Strolin^b, A. Capone^c, D. Depedis^c, U. Dore^c,
P.F. Loverre^c, D. Macina^{c,2}, M.A. Mazzoni^c, G. Piredda^c, P. Righini^c, R. Santacesaria^c

^aUniversità di Ferrara and INFN Sezione di Ferrara, Italy

^bUniversità "Federico II" and INFN Sezione di Napoli, Italy

^cUniversità "La Sapienza" and INFN Sezione di Roma, Italy

Received 27 December 1995

Abstract

We built and tested on charged particle beams the high energy-resolution calorimeter for the CHORUS experiment, which searches for $\nu_\mu - \nu_\tau$ oscillations in the CERN Wide Band Neutrino Beam. This calorimeter is longitudinally divided into three sectors: one electromagnetic and two hadronic. The first two upstream sectors are made of lead and plastic scintillating fibers in the volume ratio of 4/1, and they represent the first large scale application of this technique for combined electromagnetic and hadronic calorimetry. The third sector is made of a sandwich of lead plates and scintillator strips and complements the measurement of the hadronic energy flow. In this paper, we briefly describe the calorimeter design and we show results on its response to electrons and pions, obtained from tests performed at the CERN SPS and PS. An energy resolution of $\sigma(E)/E = (32.3 \pm 2.4)\%/\sqrt{E(\text{GeV})} + (1.4 \pm 0.7)\%$ was achieved for pions, and $\sigma(E)/E = (13.8 \pm 0.9)\%/\sqrt{E(\text{GeV})} + (-0.2 \pm 0.4)\%$ for electrons.

1. Introduction

The calorimeter described in this paper, built as a component of the CHORUS detector, is the first large scale application of the technique, developed in the past few years [1], of embedding plastic scintillating fibers into a lead matrix. The fiber sectors consists of about 1500 km of 1 mm diameter fibers in the lead-to-scintillator volume ratio of 4/1, that allows for compensation and provides good energy resolution in the detection of hadrons. Some of the 414 modules which make up the calorimeter were tested with electron and muon beams prior to the installation, and the results of these measurements have been previously reported [2]. The whole calorimeter was then tested with electrons, muons and pions.

After a brief description of the calorimeter design and

construction, we present here experimental results on the detector response to electrons and pions.

CHORUS started to take data in April 1994 in the CERN Wide Band Neutrino Beam, and the calorimeter operated successfully during the first two years of data taking.

2. Calorimeter design

The CHORUS experiment [3] searches for $\nu_\mu - \nu_\tau$ oscillations in the CERN SPS Wide Band Neutrino Beam. It uses nuclear emulsions to directly observe τ decays, produced by charged current interactions of ν_τ s, to be extracted out of a large background of ordinary ν_μ interactions. The events to be scanned in the emulsions are selected on the basis of kinematical variables, measured by means of electronic detectors. Such a selection is more efficient if the hadron shower following the neutrino interaction is measured with high angular and energy resolution. In order to detect the τ muonic decay, it is also necessary to efficiently track throughgoing muons in the

¹ Now at Università di Cagliari and Sezione INFN, Cagliari, Italy.

² Now at CERN, Geneva, Switzerland.

* Corresponding author. Address: CERN, PPE Division, 1211 Geneva 23, Switzerland.

Table 1
Calorimeter design features

	EM	H1	H2	Total
Dept: $X_0(\lambda_{int})$	21.5 (0.78)	55.2 (2.0)	67.1 (2.44)	143.8 (5.22)
Number of planes	4	5	5	14
Number of modules	124	200	90	414
Module dimensions (cm ³)	4 × 8 × 262	8 × 8 × 335	10 × 20 × 369	–
PM per module	4	2	4	–
Total number of PM	496	400	360	1256
PM type	Hamamatsu R1355/SM	Thorn-EMI 9839A	Thorn-EMI 9839A	–
Fibers/strips type	Kuraray SCS-F81	Bicron BCF-12	Bicron BC-408 (strips)	–
Number of fibers/strips	93000	310800	900	–
Total fibers/strips length (km)	283	1165	3	–
Pb weight (tons)	9.7	42	60	111.7

calorimeter and to match their trajectories with those determined by the other detectors of the apparatus.

A description of the design and construction of the calorimeter for the CHORUS experiment can be found in Ref. [2], where we also presented the response of groups

of modules to electrons of different momenta. We simply outline here the main design features, summarized in Table 1. An isometric view of the detector is shown in Fig. 1.

The calorimeter is arranged in elements (modules) to form planes oriented orthogonally to the beam, alternately

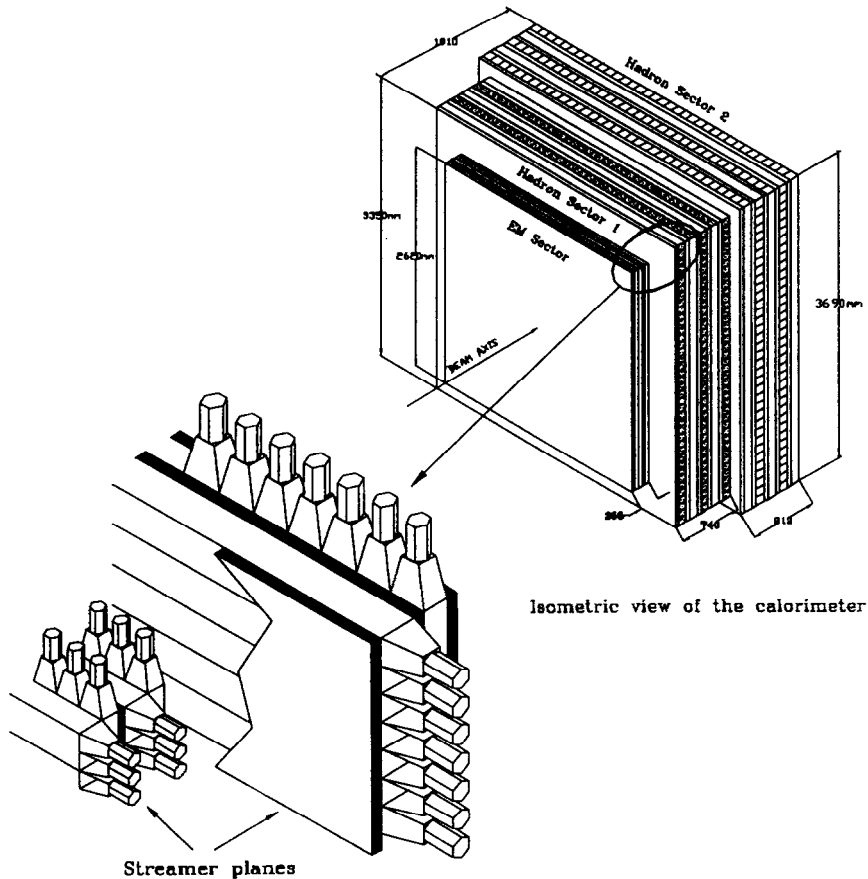


Fig. 1. Isometric view of the calorimeter.

with horizontal and vertical modules. This structure is mainly motivated by the necessity of providing muon tracking. This is the main difference with respect to the original SPACAL geometry [1], where the modules have fibers parallel to the beam direction, and the signals are collected at the back of the calorimeter. The module width orthogonal to the beam is made to be smaller than the size of the average hadron shower, to allow for reconstruction of the hadronic energy flow with adequate accuracy.

The calorimeter consists of three sectors with decreasing granularity (EM, HAD1 and HAD2). The first one measures the electromagnetic component of the events, while the other two complete the measurement of the hadron showers. The average interaction length [4] of the calorimeter is 21 cm, its radiation length 0.72 cm; the effective Moliere radius is 2 cm and the density of the modules 9 g/cm^3 . The total calorimeter thickness is about 5.2 interaction lengths (144 radiation lengths), sufficient to contain 99% of the shower induced by a $5 \text{ GeV}/c$ pion. It should be noted that about 90% of the hadrons produced in the neutrino interactions have momentum less than $5 \text{ GeV}/c$.

The EM and the HAD1 sectors (2.8 interaction lengths altogether) are made of scintillating fibers and lead, while HAD2 is a sandwich of lead and scintillating strips. The transverse structure of the calorimeter allows light collection by photomultipliers (PMs) on both sides of the module, thus reducing the effects of light attenuation in the scintillator [2].

Sets of limited streamer tube planes are inserted between the horizontal and the vertical planes for tracking purposes; they are arranged in pairs with horizontal and vertical wires. The number of planes is 22, with a total of about 7500 wires read out in digital mode.

3. Module design

Two horizontal and two vertical planes, each of 31 modules, compose the electromagnetic sector EM. Individual modules are built by piling up extruded layers of grooved lead and positioning plastic scintillating fibers in the grooves (Fig. 2). The groove diameter is 1.1 mm and the layer thickness 1.9 mm; the material, the same as for the HAD1 and HAD2 modules, is 99% lead and 1% antimony, to improve the mechanical properties. A module consists of a pile of 21 layers, 2620 mm long and 82.4 mm wide, and 740 fibers, each of 1 mm diameter and 3050 mm long. On either side of the module, fibers are assembled in two hexagonal bundles, defining two different readout cells with about $40 \times 40 \text{ mm}^2$ cross section. Each of the fiber bundles is coupled to a 1 in. PM via a plexiglas light guide. The module is held together by a steel box.

The HAD1 sector consists of five planes (three horizontal and two vertical). A plane is formed by 40 modules, each made of 43 extruded layers of lead identical in width

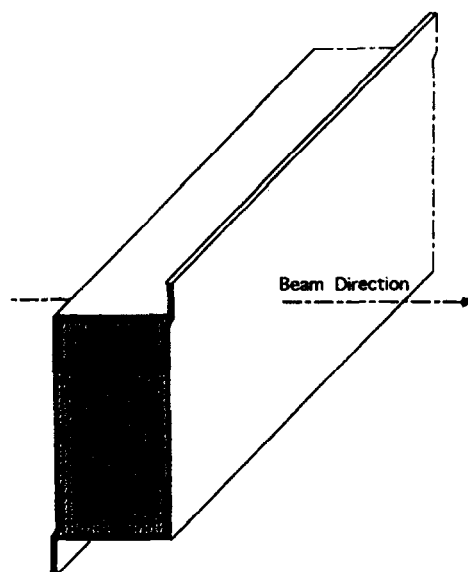


Fig. 2. View of an EM module.

and groove size to those used for the EM sector, but with a length of 3350 mm. The scintillating fibers have 1 mm diameter and 3810 mm length, with a total of 1554 fibers per module. Fibers are collected at both ends in a hexagonal bundle coupled via a light pipe to a 2 in. PM.

The HAD2 sector also consists of five planes (three vertical and two horizontal) with 18 modules each, making a total of 90 modules. Each module is constructed by superposing five alternate layers of one lead bar ($3690 \times 200 \times 16 \text{ mm}^3$) and two adjacent scintillator strips ($3714 \times 100 \times 4 \text{ mm}^3$ each), packed into a stainless steel box open at both ends (Fig. 3). Each of the two groups of five scintillators is coupled to 2 in. PMs at both ends via plexiglas light guides; therefore, a single module is seen by a total of four PM tubes, and contains two cells.

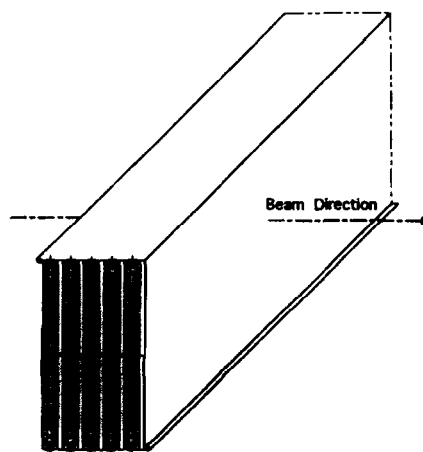


Fig. 3. View of a HAD2 module.

4. Experimental setup and data

The main measurements were performed during the autumn of 1993 in the X9 test beam at the CERN SPS. The beam line is almost parallel to the neutrino beam axis. The calorimeter, mounted on rails, can be shifted about 4 m sideways from its nominal position to meet the test beam. The setup is shown in Fig. 4.

Coincidences between the scintillation counters $T_1 \cdot T_2 \cdot T_3$ provided the main trigger. The signal from the halo counter was used off-line to reject events initiated upstream of the calorimeter. The particle impact point on the calorimeter was determined by means of the counters F_1 and F_2 , each made of four scintillators with dimensions of $1 \times 1 \times 8 \text{ cm}^3$ (fingers), placed orthogonal to the beam line in the horizontal and vertical directions respectively. In this way, their coincidence defined a matrix of 16 impact regions of 1 cm^2 .

Electron data were taken with pure beams from 2.5 to 10 GeV/c, while pions came from mixed electron/pion beams from 3 to 20 GeV/c. A nitrogen Cherenkov counter placed upstream in the beam line gave the electron/pion separation. In the energy interval explored by our measurements, the residual electron contamination of the pion sample was $\sim 2\%$. Muons were rejected off-line by exploiting the unambiguous signature given by the calorimeter itself. Fig. 5 shows the features of muon and pion events in a lego plot where the total pulse-height is plotted against the total number of hit PMs.

The analog signal of the 1256 photomultipliers of the calorimeter was digitized by dual-range 8-bit ADCs. The nominal ratio of the conversion factors for the two ADCs (high/low sensitivity) was set to 20 for all the channels: the actual value of this ratio for each ADC was determined experimentally by means of cosmic ray events. The ADC integration gate was 220 ns long, enough to contain the pion signal tails. We also took some data with a longer gate (300 ns); no difference was found in terms of calorimeter performance (linearity and energy resolution).

In order to study in more detail the stability and the uniformity of response, a further beam test was performed in April 1995 in the same location and with a similar setup. For this purpose, an additional fiber detector, lent to us and set up by the FAROS Collaboration [5], was used to define the beam impact point on the calorimeter with good space accuracy ($\sim 1 \text{ mm}$).

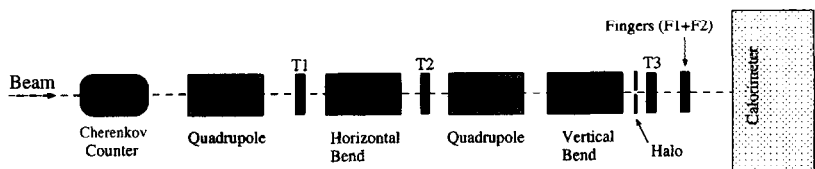


Fig. 4. SPS experimental setup (not to scale).

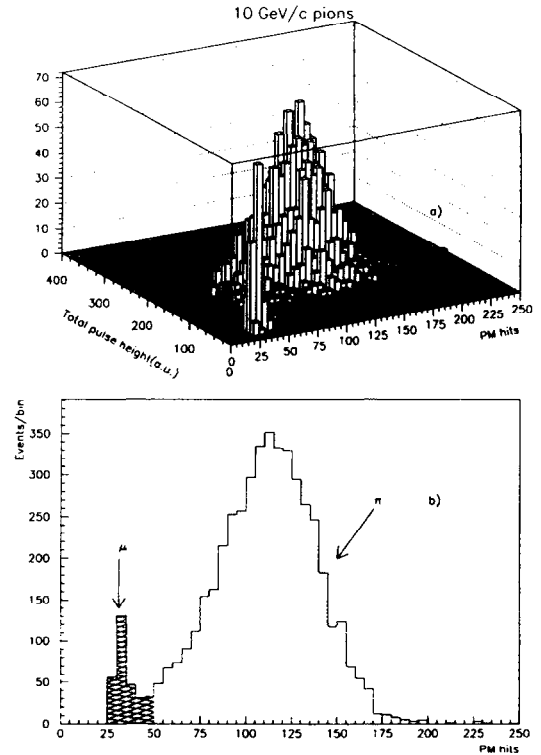


Fig. 5. (a) Lego plot of the total number of active PMs versus the total calorimeter pulse height; (b) projection: the total number of active PMs.

5. Signal equalization and sector intercalibration

Three sequential steps are needed for the determination of the calorimeter response: first, within each sector, the *equalization* of the signals from each individual PM; then the *intercalibration* among different sectors; and, finally, the overall energy calibration.

The equalization of signals from modules of the same type is performed by means of penetrating cosmic rays. An equalization constant is computed for each PM by selecting cosmic muons crossing the central region of the modules ($\pm 10 \text{ cm}$), and correcting for the effective track length.

The number of collected cosmic events is large enough to keep the statistical error on each equalization constant at the $\pm 5\%$ level. Systematic effects due to the time depen-

dence of the PM gain and to the position dependence of the energy spectra for the selected muons were also studied, the latter being due to the variable amount of material crossed by the muons before entering the module. The two combined effects account for less than 3% of the total uncertainty.

A typical pulse-height distribution of one module, for example of the HAD1 sector, is shown in Fig. 6a. A similar shape is obtained by summing the signals of all the modules of HAD1 after calibration; no significant widening of the curve is observed (Fig. 6b), thus giving us confidence in the reliability of the method.

To combine the signals of the three different sectors, two intercalibration constants are needed, namely those of HAD1 and HAD2 relative to EM. These constants are determined experimentally using pions interacting at different calorimeter depths.

Given that the response of each sector to a certain amount of deposited energy must be the same, one can select events where the shower is fully contained in two consecutive sectors A and B; therefore, the energy responses of A and B (S_A, S_B) are related to the relative intercalibration factor $\alpha_{B,A}$ by the linear equation

$$S_A + \alpha_{B,A} S_B = E_{\text{shower}}$$

E_{shower} is the shower energy, related to the pion energy by the relation

$$E_{\text{shower}} = E_{\pi} - \frac{dE}{dx} \Delta X,$$

which implies a correction for the pion energy loss before interacting at the depth ΔX . In Fig. 7 we show, as an example, S_{HAD1} as a function of S_{HAD2} for pions of given

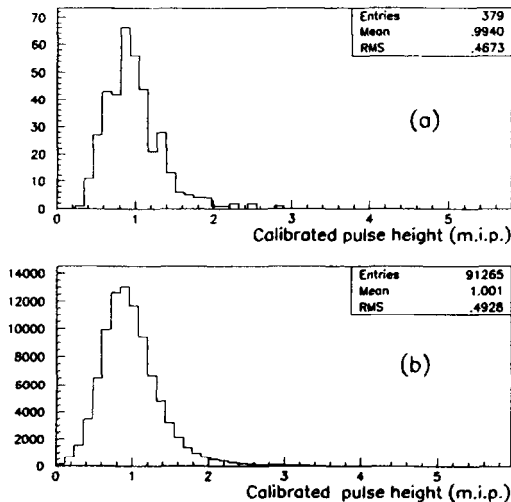


Fig. 6. (a) Typical signal distribution induced by cosmic rays in a HAD1 module; (b) the same distribution for the whole HAD1 sector.

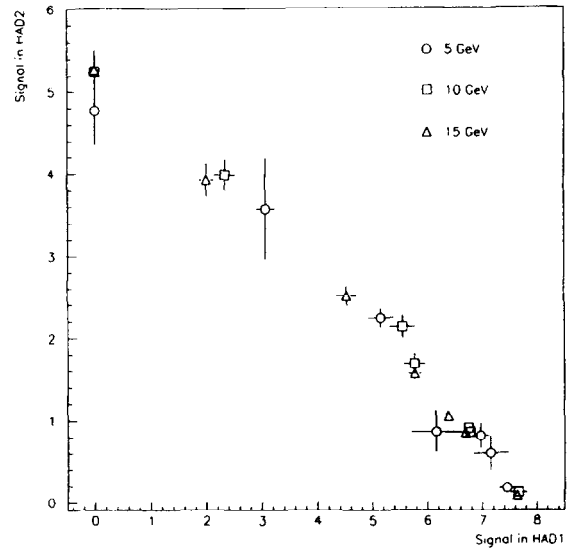


Fig. 7. Energy deposited in HAD2 as a function of the energy deposited in HAD1 by 5, 10 and 15 GeV/c pions interacting at different depths in the calorimeter. A straight line fit to the points allows to determine the intercalibration constant between the two sectors.

momentum interacting at different depths. A linear fit to the points allows the determination of the constant of calibration between the two sectors. This procedure is repeated for several beam momenta. As expected, the parameters of the fit are, within the errors, independent of the pion energy. With this method we can determine directly

$$\alpha_{\text{HAD1,EM}} = 2.34 \pm 0.06,$$

and

$$\alpha_{\text{HAD2,HAD1}} = 1.40 \pm 0.02,$$

which leads to

$$\alpha_{\text{HAD2,EM}} = 3.28 \pm 0.10.$$

It turns out that compatible numbers may be obtained by minimizing the energy resolution for pion-induced showers, but the approach described was preferred to avoid any bias.

It should be noted that the mean thicknesses of active material along the beam direction for HAD1 and HAD2, normalized to the EM value (2.1 and 2.5), do not account for the different geometries and sampling frequencies. Therefore these values are not expected to be appropriate as intercalibration constants for (hadron) showers.

6. The calorimeter signal

The calorimeter response to the incoming particle(s) is determined by adding up the energy deposited in all the modules, once the equalization and intercalibration pro-

cedures described in Section 5 have been performed. As noted before, each readout cell is equipped with a PM at each fiber (strip) end, in order to reduce the influence of the light attenuation in the scintillator. This leads to different possible definitions of the module signal, according to the way the two PM signals (L and R) are combined. In particular, one can use the arithmetic or the geometric mean:

$$S_a = \frac{S_L + S_R}{2}, \quad S_g = \sqrt{S_L \times S_R}.$$

Under the assumption of a single hit per module and exponential light attenuation in the fibers (strips), as found in Ref. [2], the geometric mean yields a value for the module response (and hence for the energy) which is independent of the hit position x along the module with length L :

$$S_L = A e^{-x/\lambda}, \quad S_R = A e^{-L-x/\lambda} \rightarrow S_g = A e^{-L/2\lambda}$$

A small position dependence arises in case of multiple hits.

A correction must be applied for the channels which are noisy or dead. The signal of the other PM of the same cell is used in this case, after correction for the light attenuation corresponding to the hit position. During the beam test data-taking, only about 10 channels needed this correction.

In Fig. 8 we show the calorimeter signal distribution produced by 10 GeV/c negative pions. Each entry corresponds to the calibrated sum of the response of all the molecules, as obtained computing the geometric mean. The shape is Gaussian, indicating that both the calibration and intercalibration procedures do not introduce any appreciable bias in the determination of the overall calorimeter

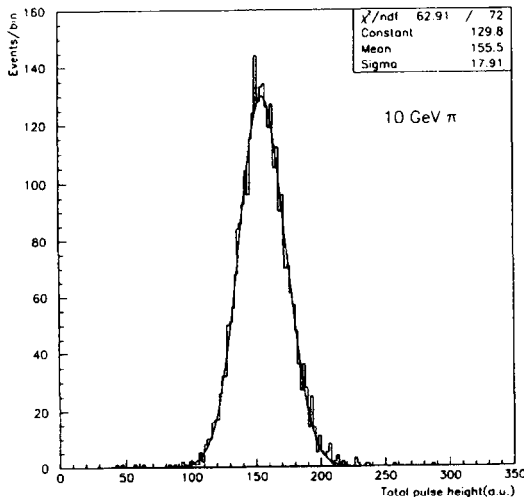


Fig. 8. Calorimeter response to 10 GeV/c pions.

response. All the results presented in this paper were obtained following the same described procedure.

7. Monte Carlo simulation

A Monte Carlo simulation of the calorimeter has been performed in order to study its response to different kinds of incoming particles and to showers initiated by neutrino interactions. Calorimeter behaviour was simulated by reproducing the full geometry, down to the details of the scintillating fiber (strip) and lead structure of the different modules. Direct tracking of charged and neutron particles is performed, including all types of secondaries at least down to 10 keV. All electromagnetic and hadronic processes (elastic and inelastic) are taken into account.

The task has been accomplished by using the GEANT 3.21 package [6], together with FLUKA [7] for the hadronic reactions, and MICAP [8] to deal with low energy (lower than 20 MeV) neutron interactions down to the thermal region of a few eV kinetic energy. Many other effects related to the actual digitization and readout of the calorimeter are included:

- the Birk's law related to the light yield of the scintillator;
- the attenuation length of the light in the scintillator simulated using the experimental values for the different types of modules;
- the signal resolution, parameterized according to

$$\frac{\sigma(s)}{s} = \sqrt{\frac{\alpha}{s} + \beta}$$

where s is the light intensity at the photocathode. The constants α and β are determined experimentally by comparing the output of the two PMs connected to the same module. The first term under the square root represents the photoelectron statistics, while β , found to be negligible, includes all the imperfections in the light collection:

- the actual ADC time integration gate (220 ns) is used to cut the tails of the thermal neutron energy deposition;
- the dual range ADC digitization is reproduced as in the real case.

Fig. 9 shows a typical Monte Carlo event induced by a 3 GeV/c pion.

8. Response to electrons

The electron response was studied for different SPS beam momenta, in the range from 2.5 to 10 GeV/c, relevant for the CHORUS experiment. For each momentum, a Gaussian fit was performed to the distribution of the calorimeter signal (Fig. 10), as defined in Section 6. The mean value S of the Gaussian is plotted in Fig. 11 versus the beam momentum P .

The measured points lie on a straight line up to 10 GeV/

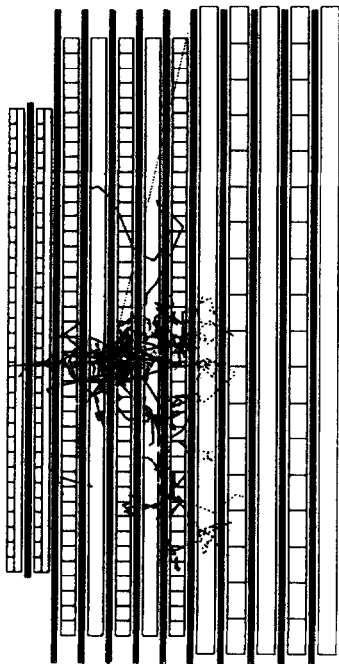


Fig. 9. Monte Carlo simulation of a 3 GeV/c pion event; solid (dashed) lines represent charged (neutral) particles.

c, where electronics saturation tends to reduce the calorimeter signal. This effect is due to the small spatial dimensions of the electromagnetic showers, such that a large fraction of the energy can be released in a single EM module. This does not happen for hadron or neutrino induced events, where many modules share the incident energy.

The result of a linear fit (also shown in Fig. 11) performed in the interval from 2.5 to 5 GeV/c indicates

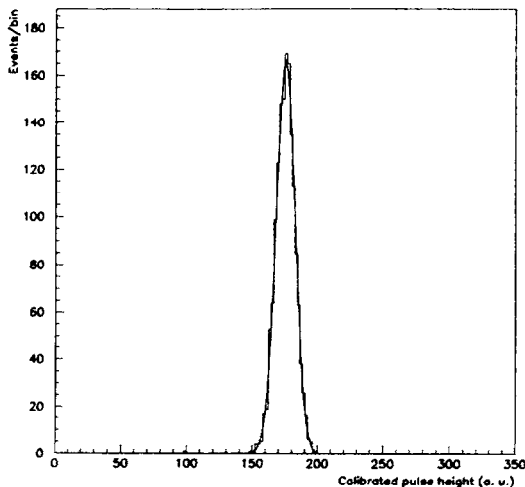


Fig. 10. Calorimeter response to 10 GeV/c electrons.

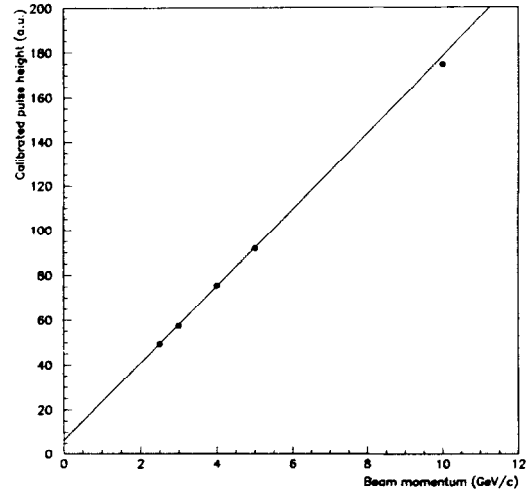


Fig. 11. Calorimeter response as a function of the electron momentum.

that extrapolation to zero pulse height leads to a *negative* value of the momentum:

$$S = (17.2 \pm 0.3) \times P(\text{GeV}/c) + (6.4 \pm 0.9).$$

The above result is in agreement with our previous analysis on the electromagnetic response of single calorimeter modules, tested on the same beam line [2]. It is consistent with the actual value of the beam momentum being $370 \pm 50 \text{ MeV}/c$ higher than the nominal value.

The electromagnetic response of the calorimeter and its linearity have been thoroughly investigated by simulation. Monte Carlo predictions give a linear response of the detector to electrons, as well as to photons, and no offset is expected. As pointed out in Ref. [2], the origin of this experimental offset may depend upon the SPS beam momentum calibration.

In order to solve this problem, independent measurements were done at the CERN PS. A setup consisting of four EM and one HAD1 modules, able to contain electromagnetic showers, was exposed to low momentum electrons from the T11 beam, ranging from 1 to 7 GeV/c. The results indicate that the extrapolation to zero calorimeter pulse height does indeed lead to a momentum compatible with zero (intercept equal to $+40 \pm 20 \text{ MeV}/c$), supporting the conclusion of a calibration shift of the SPS X9 beam momentum. These results are shown in Fig. 12, together with the SPS points corrected for the 370 MeV/c offset; the agreement between the two sets of data is excellent.

The following (corrected) relation is then obtained for the energy dependence of the electromagnetic response:

$$S = (17.2 \pm 0.3) \times P(\text{GeV}/c) - (0.14 \pm 0.96). \quad (1)$$

The energy resolution $\sigma(E)/E$ is plotted in Fig. 13 as a

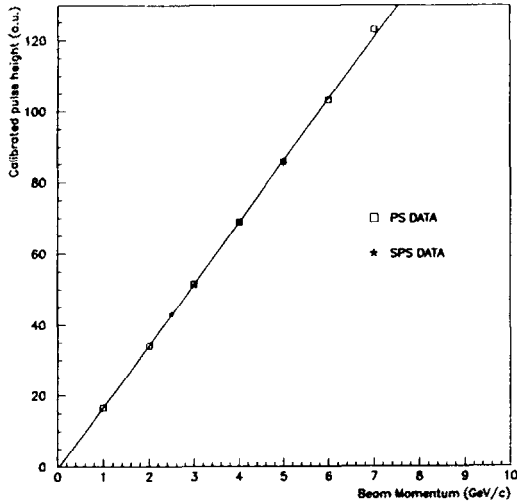


Fig. 12. Electron response for the PS setup. The SPS points are also shown, corrected for the 370 MeV/c momentum shift.

function of the electron energy. The energy dependence of the resolution is well fitted by the usual function:

$$\frac{\sigma(E)}{E} = \frac{(13.8 \pm 0.9)\%}{\sqrt{E(\text{GeV})}} + (-0.2 \pm 0.4)\%$$

This result fulfils the design requirements and agrees with the Monte Carlo predictions.

We also studied the uniformity of the electromagnetic response as a function of the particle impact point on the calorimeter. Given the very limited transverse dimensions of electromagnetic showers in a lead calorimeter, we expect a reduction of the signal response to occur near the EM module edge, where no active material is present (crack).

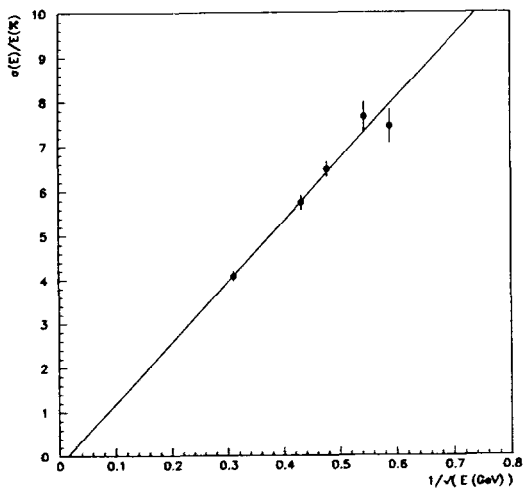


Fig. 13. Energy resolution for electrons as a function of the energy.

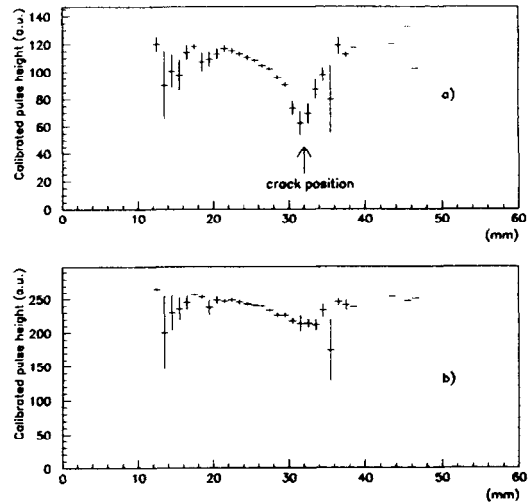


Fig. 14. (a) Energy deposition in the second EM plane as a function of the horizontal beam impact point, for 10 GeV/c electrons. The dip corresponds to the boundary between two vertical modules; (b) the corresponding total calorimeter signal as a function of the impact point.

For this analysis we used the FAROS detector to select electrons hitting the calorimeter in the crack between two adjacent (vertical) modules in the second EM plane, where showers are already developed. Fig. 14a shows the total energy released in that plane, by 10 GeV/c electrons, as a function of the impact point horizontal coordinate. One can see that, in a region 4 mm wide centered on the crack, the signal is reduced by about 25–40%, indicating that part of the shower energy is, in this case, undetected. The consequent reduction of the total calorimeter signal amounts of 5–10%, as shown in Fig. 14b. However, applying geometrical considerations, this disuniformity would affect, on average, only 2% of the electromagnetic showers. We did not use those events occurring in the crack for the previous studies on the electromagnetic response and energy resolution.

By studying electron showers developing in different calorimeter zones we estimated the disuniformity in the electromagnetic response to be of the order of $\pm 5\%$, in agreement with the design requirements.

9. Response to pions

To study the hadronic performance of the calorimeter without systematic errors caused by showers leaking at the rear of the detector, in the following analysis we selected only those events with the pion interacting in the EM section.

The pion response was studied for different beam momenta, from 3 to 20 GeV/c. The mean value S of the

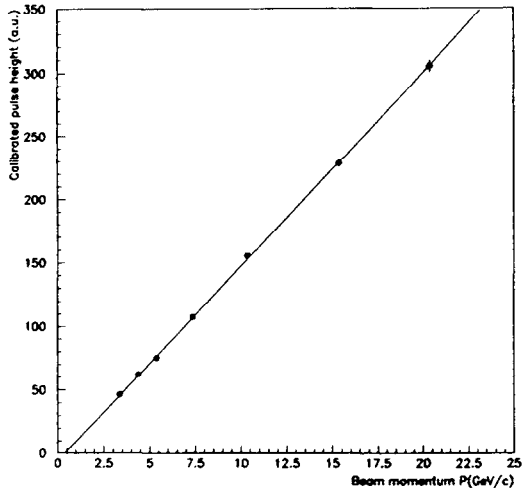


Fig. 15. Calorimeter response as a function of the pion momentum.

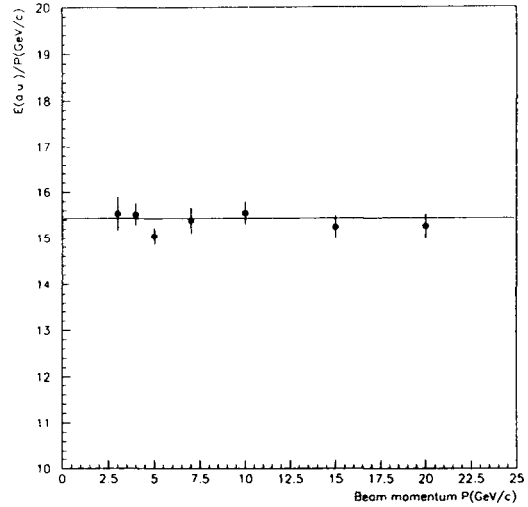


Fig. 16. Calorimeter response per unit momentum as a function of the pion momentum.

signal distribution, which is Gaussian as in the electron case, is plotted in Fig. 15 as a function of the nominal momentum P , corrected for the shift of 370 MeV/c, found with the electron data. The measured pion momentum dependence may be parameterized as:

$$S = (15.3 \pm 0.2) \times P(\text{GeV}/c) - (5.8 \pm 1.0), \quad (2)$$

which corresponds to a *positive* intercept of 380 ± 65 MeV/c. A different value of this quantity, which is expected for electrons (compatible with zero) and pions can be understood on the basis of the following considerations:

- a comparison of the response to electrons and pions of the same energy shows deviations from exact compensation ($S_{\text{electron}} > S_{\text{pion}}$). Therefore, at high momenta, the increase of the electromagnetic energy content in the hadron showers ($E_{\text{EM}}/E_{\text{TOT}} \propto \ln(E_{\text{TOT}})$) induces an energy dependent enhancement of the signal.

- At low momenta (~ 1 GeV/c), the contribution from neutral pions becomes negligible and small multiplicity processes dominate. In this case, the effect of the particle masses not converted into visible energy in the readout gate becomes visible.

Both the above effects indicate that a straight line fit to the data taken in the stated momentum range should have an intercept at a positive value of the abscissa. This is confirmed by the Monte Carlo simulation, which predicts an intercept of 340 ± 50 MeV/c. Fig. 16, where the response per unit energy is plotted as a function of the pion momentum, one finds that the calorimeter is linear within 2% in the range 3 to 20 GeV/c and that there is no evidence for saturation, even at the highest energy.

In conclusion, the SPS pion/electron linearity measurements are internally consistent and in agreement with the simulation, in the hypothesis of an offset in the nominal beam momentum.

From the Gaussian fit to the response distributions one determines the energy resolution $\sigma(E)/E$, which is plotted in Fig. 17 as a function of the pion energy. The errors assigned to each point include a systematic uncertainty of about 2% determined by applying different event selection criteria to the data, and studying pions hitting different calorimeter positions. The above uncertainty is lower than that for the electron case ($\pm 5\%$). The main reason is the larger number of calorimeter modules involved in a hadron shower. Note that a study performed with the FAROS detector, similar to the case of electrons, does not show, as expected, any *crack* effect. The energy dependence of the resolution is parameterized as:

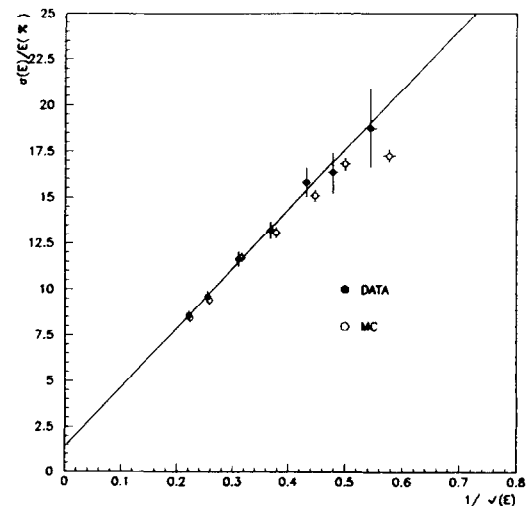


Fig. 17. Pion energy resolution as a function of the energy. The open circles show the Monte Carlo predictions.

$$\frac{\sigma(E)}{E} = \frac{(32.3 \pm 2.4)\%}{\sqrt{E(\text{GeV})}} + (1.4 \pm 0.7)\%.$$

The predictions of a Monte Carlo simulation are also shown in Fig. 17.

The experimental energy resolution can be interpreted in terms of the different energy resolutions of the fiber and strip sectors:

$$\frac{\sigma(E)}{E} = \sqrt{k(\sigma_f/E)^2 + (1-k)(\sigma_s/E)^2},$$

where k is the measured energy fraction in the fiber sector (0.89 at 10 GeV) and σ_f/E is its expected resolution ($30\%/\sqrt{E} + 0.5\%$), while σ_s/E is the resolution of the strip calorimeter alone. As an example, the above formula yields, for the experimental resolution of 11.6% at 10 GeV, an energy resolution of $60\%/\sqrt{E}$ for the HAD2 calorimeter.

The longitudinal and transverse shower development in the calorimeter is shown in Fig. 18 for a 10 GeV/c pion. Many events are superimposed to obtain the *average* behaviour. Fig. 19a shows the projection of the shower onto the transverse plane. In Fig. 19b it is shown that a cylinder containing 95% of the shower energy has a radius of about 25 cm, almost constant in the energy range explored by our measurements. This result is in excellent agreement with the Monte Carlo prediction, also shown in the figure.

The longitudinal development is presented in Fig. 20a for different pion momenta. Fig. 20b shows the fraction of energy deposited at different calorimeter depths normalized to the total calorimeter signal. In both cases, the

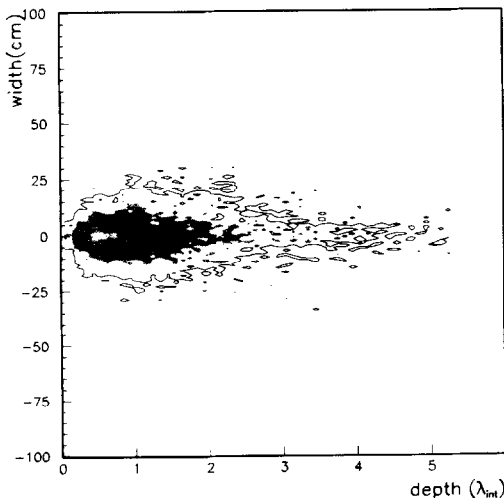


Fig. 18. Shower development for 10 GeV/c pions. Different grey zones correspond to different pulse height levels. The continuous line is 1% of the maximum intensity.

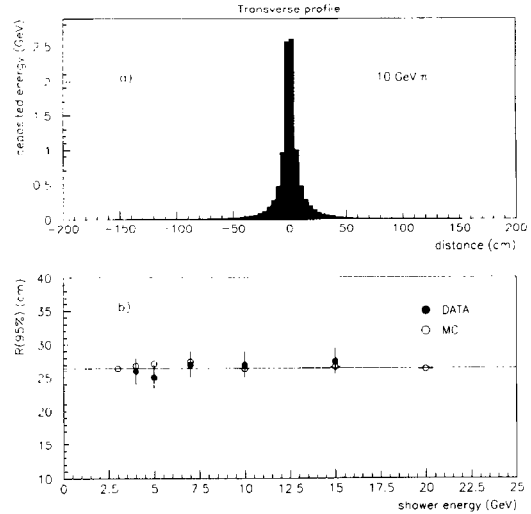


Fig. 19. (a) Shower projection onto the transverse plane orthogonal to the beam direction for 10 GeV/c pions; (b) transverse dimensions of the pions shower as a function of the energy: the black circles represent the radius around the shower axis which contains 95% of the energy. The open circles show the Monte Carlo predictions.

Monte Carlo results are also given; the comparison indicates very good agreement.

We also studied the calorimeter performance for the measurement of the shower direction. The angular resolution is determined using the center of gravity of the energy deposition in each calorimeter plane. Figs. 21a and 21b show, respectively for the two projections (the beam goes along x), the energy center of gravity distributions (per plane), induced by 10 GeV/c pions. From the knowledge of the center of gravity coordinates in the different planes, event by event one can determine the shower direction. The distributions of the fitted angle, for both projections, are shown in Figs. 22a and 22b for 10 GeV/c pions. We obtain an angular resolution of about 60 mrad (HWHM) at 10 GeV/c for the two transverse projections. The effect of the beam angular spread (<1 mrad), folded into the measurement, can be neglected. The Monte Carlo predictions, shown in the figure, are in agreement with the data³.

From the electron and pion response of the calorimeter we can determine the experimental e/π ratio. In Fig. 23 we plot the ratio of the average electron and pion calorimeter signal, computed at the same (corrected) momentum, as a function of the momentum. The systematic error, due to the response disuniformity, has been added to the statistical error. In the same figure, we also plot the ratio of the

³ A better angular resolution was obtained in CHORUS using the calorimeter information and the position of the neutrino interaction point in the emulsion target [3].

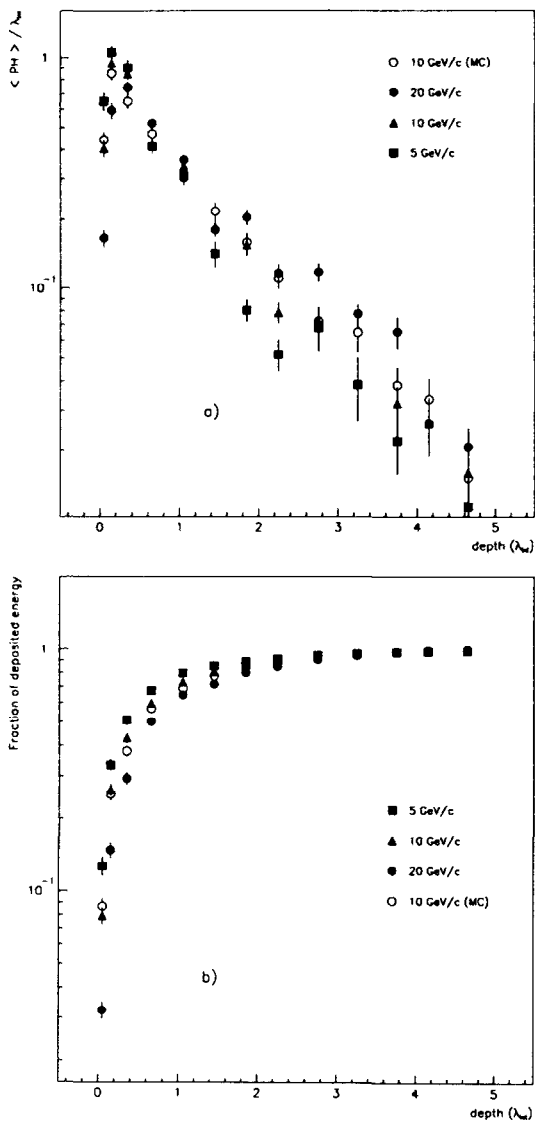


Fig. 20. (a) Longitudinal shower development for different pion momenta; (b) fractional energy deposition. The Monte Carlo simulation result is also shown for 10 GeV pions.

functions (1) and (2), describing the signal momentum dependence for electrons and pions. This measurement, performed at relatively low energy, does not allow us to compute the e/h ratio, where h is defined as the purely non-electromagnetic component of the hadron shower.

10. Conclusions

We have presented experimental results on the electron and pion response of the calorimeter for the CHORUS experiment. The calorimeter, the first large scale applica-

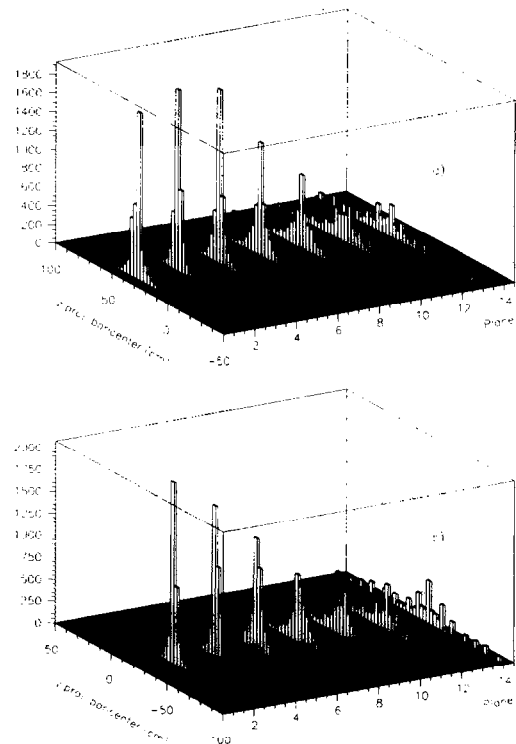


Fig. 21. Energy center of gravity distributions (per plane) induced by 10 GeV/c pions; (a) $x-z$ projection, (b) $x-y$ projection.

tion of the scintillating fiber/lead technique for integrated electromagnetic/hadronic calorimetry, was exposed to electron and pion beams in the momentum range from 2.5 to 20 GeV/c at the CERN SPS. A further test of calorimeter modules, performed at the CERN PS, allowed us to study the low energy electromagnetic response.

Electrons were studied, in the SPS beam, in the momentum range from 2.5 to 10 GeV/c. The calorimeter response was found to be linear with the momentum after applying a correction to its nominal value, as indicated by measurements performed at the CERN PS. The energy dependence of the resolution was parameterized as $\sigma(E)/E = (13.8 \pm 0.9)\% / \sqrt{E(\text{GeV})} + (-0.2 \pm 0.4)\%$.

The calorimeter response to pions was linear in the momentum range explored by the measurements, and we achieved an energy resolution of $\sigma(E)/E = (32.3 \pm 2.4)\% / \sqrt{E(\text{GeV})} + (1.4 \pm 0.7)\%$. This result is in agreement with the design features and the Monte Carlo predictions.

The shower development in the longitudinal and transverse directions was studied as a function of the beam momentum and the results are in good agreement with the Monte Carlo expectations. The comparison between the pion and electron response allowed us to measure the e/π ratio in the low momentum region.

The calorimeter has been successfully operational during the 1994 and 1995 data taking periods of the CHORUS experiments in the CERN Wide Band Neutrino Beam.

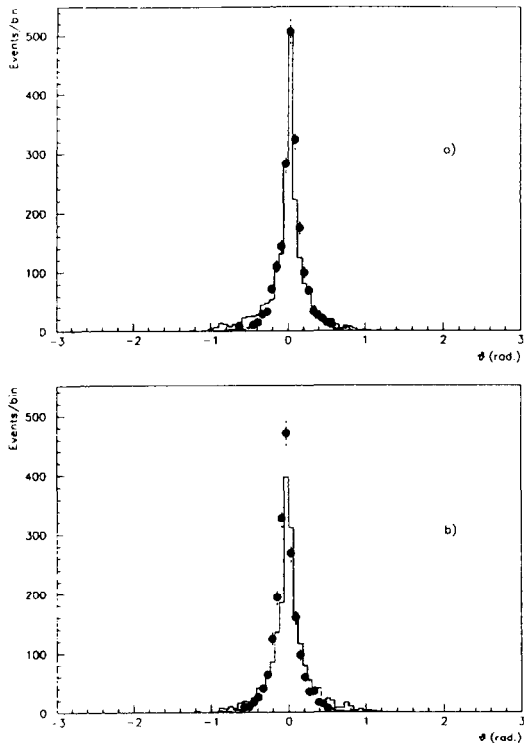


Fig. 22. Angular resolution for 10 GeV/c pions; (a) x - z projection, (b) x - y projection. The continuous line represents data events and the black circles show the results of a Monte Carlo simulation.

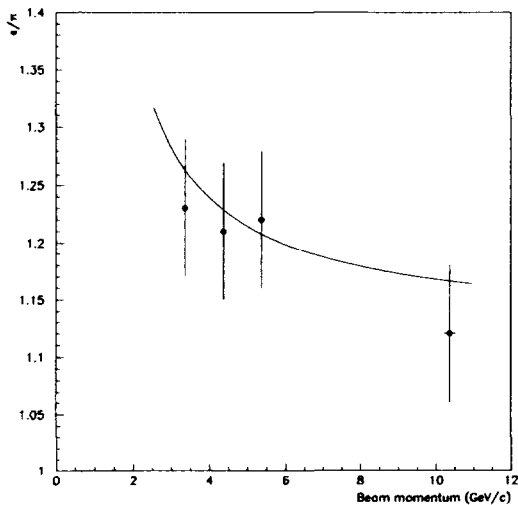


Fig. 23. e/π ratio as a function of the beam momentum. The continuous line represents the ratio of the electron and pion momentum-dependence functions.

Acknowledgements

This work was carried out with the financial support of the Italian Istituto Nazionale di Fisica Nucleare. We gratefully acknowledge the skill of our technical collaborators and engineers. In particular, we thank V. Carasiti for the design and supervision of the mechanical aspects of the whole project and G. Basti, R. Gorini and G. Passeggio for their contribution to the design. We also thank S. Bigoni, G. Bonora, F. Evangelisti, G. Improta, A. Iacofano, M. Melchiorri, R. Rocco and S. Sabbioni for their contributions in the different phases of the calorimeter assembly. The kind help of many CHORUS colleagues during the calorimeter construction and testing is also warmly acknowledged. We are indebted to L. Gatignon for the operation of the SPS X9 beam line. We finally wish to acknowledge the collaboration of A. Gurin, K.I. Kuroda, I. Manouilov and T. Yoshida in setting-up the FAROS detector, an essential tool in the study of the uniformity of response.

References

- [1] D. Acosta et al., Nucl. Instr. and Meth. A 308 (1991) 481.
- [2] S. Buontempo et al., Nucl. Instr. and Meth. A 349 (1994) 70.
- [3] M. de Jong et al., CERN-PPE/93-131.
- [4] Particle Data Group, Phys. Lett. B 239 (1990) p. III 5,6.
- [5] V. Agoritzas et al., LAPP-EXP-95-01, Proc. Int. Conf. on Advanced Technology and Particle Physics, Como, 3–7 October 1994.
- [6] CERN Program Library Long Writeup Q123.
- [7] A. Fassò et al., FLUKA 92, Proc. Workshop on Simulating Accelerators Radiation Environments, Santa Fe, 11–15 January 1993.
- [8] T.A. Gabriel and J.O. Johnson, Technical Rep. TM 10340, ORNL.